



## Selective conversion of concentrated glucose to 1,2-propylene glycol and ethylene glycol by using RuSn/AC catalysts

Jifeng Pang<sup>a</sup>, Mingyuan Zheng<sup>a,\*</sup>, Xinsheng Li<sup>a,c</sup>, Yu Jiang<sup>a</sup>, Yu Zhao<sup>a</sup>, Aiqin Wang<sup>a,b</sup>, Junhu Wang<sup>a</sup>, Xiaodong Wang<sup>a</sup>, Tao Zhang<sup>a,b,\*</sup>

<sup>a</sup> Dalian Institute of Chemical Physics, Chinese Academy of Sciences, Dalian, 116023, China

<sup>b</sup> State Key Laboratory of Catalysis, Dalian, 116023, China

<sup>c</sup> University of Chinese Academy of Sciences, Beijing, 100049, China



### ARTICLE INFO

#### Keywords:

RuSn catalyst  
Concentrated sugar  
1,2-propylene glycol  
Ethylene glycol  
Hydrogenolysis

### ABSTRACT

A series of RuSn/AC catalysts with 5% Ru and 1–6% Sn loadings were synthesized for converting concentrated (10 wt%) sugars to 1,2-propylene glycol (1,2-PG) and ethylene glycol (EG) in a semi-continuous autoclave reactor. The catalysts structure and the product distributions are found to be highly dependent on the tin loading. At tin contents below 2%, RuSn alloy was formed coexisting with small amounts of highly dispersed SnO<sub>2</sub> in the catalyst, and hexitols were the main products due to the high activity of catalysts for hydrogenation. At a tin content above 5%, more SnO<sub>2</sub> species were present and covered RuSn alloy particles, leading to notable amounts of humins in the reaction due to the depressed hydrogenation activity. As for the optimal catalyst of 5%Ru3%Sn/AC, 77% of tin formed RuSn alloy with ruthenium and 23% of tin existed in the form of highly dispersed SnO<sub>2</sub> under reaction conditions. The catalyst gave 25% and 26.9% yields of 1,2-PG and EG in the glucose conversion at 513 K for 10 min. The glycols yield was insensitive to the feeding rate of glucose, which could be increased to 10 mL/min with a glycols productivity of nearly 180 g L<sup>-1</sup> h<sup>-1</sup>. The catalysts structure and reaction networks were proposed according to pseudo *in situ* characterizations and conditional experiments. The highly dispersed SnO<sub>2</sub> was effective to sugar isomerization and the RuSn alloy played the major role in retro-aldol condensation and hydrogenation reactions. Over the 5%Ru3%Sn/AC catalyst, the rates of cascade reactions of isomerization, retro-aldol condensation and hydrogenation matched well due to the balanced activity of RuSn alloy and highly dispersed SnO<sub>2</sub>, which afforded a high yield of 1,2-PG and EG.

### 1. Introduction

1,2-propylene glycol (1,2-PG) and ethylene glycol (EG) are important glycols, widely used for the synthesis of polyesters. In the past five years, the consumption of glycols increased at a rate of 5% annually and reached ca. 30 million tons owing to the rapid development of textile, beverage package and unsaturated resin production [1]. Currently, 1,2-PG and EG are mainly synthesized from fossil resources derived propylene and ethylene [2]. Due to the fossil energy depleting and its consumption caused environmental issues, it is highly attractive to synthesize glycols from renewable biomass [3–6].

Cellulose is the major component in lignocellulosic biomass, which is suitable to be used as a feedstock for the synthesis of glycols via catalytic processes. Tungsten based catalysts were found to be highly active for the one-pot conversion of cellulose to EG [7,8]. Over Ni-W<sub>2</sub>C/AC catalysts, the EG yield reached 61% at 100% cellulose conversion

[9]. By adjusting the dispersion and chemical states of tungsten sites, the EG yield was promoted to ca. 76% over bimetallic Ni-W/SBA-15, WC<sub>x</sub>/MC (mesoporous carbon), Ru/WO<sub>3</sub> (nanosheets) and 3Al-15W-3Ni-TUD-1 (zeolites) catalysts [10–13]. Over binary catalysts of Ni(Ru)-H<sub>2</sub>WO<sub>4</sub>, ca. 60% EG yield was obtained in more than twenty times run [14,15]. The reaction selectivity can be tuned between EG and 1,2-PG. Over a mixed catalyst of 50%WO<sub>3</sub>/Al<sub>2</sub>O<sub>3</sub> + C<sub>act</sub>, the main product was 1,2-PG with 40.9% selectivity at 21.2% cellulose conversion [16]. Some other transition metal catalysts, including Ni/ZnO, CuCr, Ni-La(III) and Ru/NbOPO<sub>4</sub>, also showed considerable activities for the conversion of cellulose to glycols [17–20]. These endeavors greatly promote the conversion of biomass to important chemicals.

Monosaccharides, typically glucose and fructose, are the key intermediates for glycols production. They can be produced from lignocellulosic biomass through acid or enzyme hydrolysis [21–23]. Compared to the solid cellulosic biomass, the conversion of soluble

\* Corresponding authors at: Dalian Institute of Chemical Physics, Chinese Academy of Sciences, Dalian, 116023, China

E-mail addresses: [myzheng@dicp.ac.cn](mailto:myzheng@dicp.ac.cn) (M. Zheng), [taozhang@dicp.ac.cn](mailto:taozhang@dicp.ac.cn) (T. Zhang).

sugars is more convenient to be handled in terms of high concentration of feedstock and continuous operation, which endow the process with much higher efficiency [24,25]. Tungsten based catalysts have been used for glucose conversion to EG. Over a binary catalyst of ammonium metatungstate and Ru/AC, the EG yield reached 60% at the glucose concentration of 5–10% in a semi-continuous autoclave reactor [26]. In another study, 66% EG yield was obtained over nickel promoted tungsten carbide catalysts in a fed-batch reaction system, giving a volume productivity of nearly 300 g<sub>EG</sub> L<sup>-1</sup> h<sup>-1</sup> [27]. In a fixed-bed reactor, 1,2-PG was obtained with 60.8% selectivity at 92.2% glucose conversion over Pd-WO<sub>3</sub>/Al<sub>2</sub>O<sub>3</sub> catalysts [28,29]. In addition, Cu-Cr catalysts by the aid of Ca(OH)<sub>2</sub> were also active for glucose conversion, giving 52.8% 1,2-PG yield in a two-step process [30]. Over a Pd/C-Zn/ZnO catalyst, 33.3% yield of 1,2-PG was obtained [31].

Recently, tin based catalysts were found to be highly active for sugars conversion [32,33]. Sn-zeolite catalysts with tin incorporated into the framework of zeolite demonstrated high activity for C–C bonds cleavage in sugars conversion [32,34–36]. Additionally, the SnO<sub>x</sub> particles in Pt-SnO<sub>x</sub>/Al<sub>2</sub>O<sub>3</sub> catalysts promoted the conversion of cellulose to C<sub>2</sub> and C<sub>3</sub> compounds at a Sn/Pt atomic ratio larger than 2.1 [37]. Our recent study found that tin species played important roles in cellulose conversion to glycols over Ni-Sn catalysts, and yields of EG and 1,2-PG can be tuned to some extent by adjusting the valence state of tin [38]. Herein, we developed an effective RuSn/AC catalyst for the conversion of concentrated monosaccharides in a semi-continuous autoclave reactor. 1,2-PG and EG were obtained at an overall glycols yield of 67% with a high productivity of 180 g L<sup>-1</sup> h<sup>-1</sup>. The structure of bimetallic catalysts was characterized to illustrate the chemical states of Ru and Sn on the catalysts. Effects of tin loading and reaction parameters on glycols yield were investigated to optimize the glycols yield. The reaction pathway and the role of active sites for glycols production were proposed according to the conditional experiments and catalyst characterizations.

## 2. Experimental

### 2.1. Catalyst preparation

RuSn/AC catalysts were prepared by an incipient-wetness impregnation method [39]. Take the 5%Ru3%Sn/AC catalyst as an example, 2 g 5%Ru/AC (DIPC produced) was impregnated with an aqueous solution containing 0.178 g SnCl<sub>4</sub>·4H<sub>2</sub>O (accounting for 3% Sn loading). The mixture was maintained at 298 K for 12 h and dried at 393 K for 12 h, and then reduced in a H<sub>2</sub> flow at 523 K for 1 h. Prior to exposure to air, the as-prepared catalyst was passivated in a flow of 1% O<sub>2</sub>/N<sub>2</sub> for 12 h at room temperature. For comparison, 3%SnO<sub>x</sub>/AC catalysts were prepared by the impregnation method, and further reduced under the same conditions as that for RuSn/AC catalysts.

### 2.2. Catalyst characterization

X-ray diffraction (XRD) patterns were obtained by using a PANalytical X'Pert-Pro powder X-ray diffractometer, operated at 40 kV and 40 mA with Cu K $\alpha$  monochromatized radiation ( $k = 0.1541$  nm) at a scan speed of 5°/min in the angular range of 10–80°. Before analysis, samples were crushed to powders smaller than 80 meshes and loaded into a glass slide.

Specific surface areas and pore volumes of Ru/AC and RuSn/AC catalysts were characterized by using a Micromeritics ASAP 2020 system. Approximately 0.1 g of each sample was degassed at 393 K for 3 h to remove the adsorbed water, and at 523 K for 3 h to get a clean surface of catalysts for nitrogen adsorption. The treated sample was measured at 77 K using nitrogen as the adsorbent. Surface areas were determined by the BET method. Pore volumes and average pore diameters were calculated using the BJH method.

Temperature programmed reduction (TPR) experiments were

carried out on a Micromeritics AutoChem II 2920 automated catalyst characterization system equipped with a thermal conductivity detector (TCD). About 0.1 g of unreduced catalyst was loaded in a U-shaped quartz reactor and pretreated with air at 423 K for 1 h to remove the adsorbed water. After cooling to room temperature, the flowing gas was switched to 10 vol% H<sub>2</sub>/Ar, and the catalyst was heated to 873 K at a ramp rate of 10 K/min. During the TPR process, on line mass spectrometry (MS) was operated to monitor the gaseous products.

High-resolution transmission electron microscopy (HRTEM), and energy dispersive X-ray spectroscopy (EDS) elemental mapping were performed on a JEM-2100 F microscopy, operated at a voltage of 200 kV. The samples were dispersed in ethanol for 5 min using an ultrasonic bath, and then mounted on carbon coated Cu grids followed by slow evaporation of the solvent at room temperature. Particle sizes were measured with the help of the image software. For each sample more than 100 particles were measured using two to four different images per sample.

X-ray photoelectron spectroscopy (XPS) of RuSn/AC catalysts were conducted on an ESCALAB 250Xi spectrometer using Al K $\alpha$  ( $\lambda = 1486.6$  eV) X-ray source with pass energy of 20 eV, and base pressure of analysis chamber less than  $1 \times 10^{-8}$  Pa. The spectra of as-prepared RuSn/AC catalysts were directly collected without further reduction. To obtain the spectra of the freshly reduced catalyst, the sample was treated at 523 K in hydrogen for 2 h and then cooled to room temperature without exposure to air for the XPS measurement. Binding energy (BE) values were referenced to the binding energy of the C 1 s core level at 284.6 eV.

The <sup>119</sup>Sn Mössbauer spectra of catalysts were collected at room temperature using <sup>119</sup>Sn in the BaSnO<sub>3</sub> as an emitter, and the isomer shift (IS) was given with respect to the centroid of BaSnO<sub>3</sub> at room temperature. All spectra were computer-fitted using the Lorenzian function with a least-squares fitting procedure.

### 2.3. Catalytic conversion of sugars

Catalytic conversion of sugars was carried out in a semi-continuous reaction system following our previous report (see supplementary information, Scheme S1) [26]. Typically, certain amounts of catalysts and 20 mL of water were charged in a 100 mL stainless-steel autoclave (Parr Instrument Co.). The reactor was then flushed with 0.2 MPa hydrogen for 6 times and filled with 5 MPa hydrogen. The mixture was stirred at a rate of 800 rpm and heated to desired reaction temperatures. Then, 20 mL of 10 wt% sugar solution was fed into the reactor by a high pressure pump (Elite MP10) and reacted for 10 min. To monitor the reaction intermediates over different catalysts, products were *in situ* sampled from the autoclave (with an inner filter screen, 300 mL, Parr), and quenched to room temperature for analysis. For stability tests, the RuSn/AC catalyst was filtered and rinsed with deionized water for 3 times, and then put into the reactor for the next run.

The liquid products were analyzed by using an Agilent 1200 HPLC equipped with a Shodex Sugar SC1011 column and a refractive index detector, and water was used as a mobile phase. Gaseous products were analyzed by using an Agilent 6890 N gas chromatography equipped with a TDX-1 column and thermal conductivity detector. The product yield was calculated based on the carbon mole ratio.

The products yield and sugars conversion were calculated as follows:

$$\text{Yield (\%)} = \frac{\text{mol of carbon in the target products}}{\text{mol of carbon in the substrate fed into the reactor}} \times 100\%$$

$$\text{Conversion (\%)} = \frac{\text{mol of carbon in the converted substrate}}{\text{mol of carbon in the substrate fed into the reactor}} \times 100\%$$

Volumetric productivity of glycols was calculated by dividing the total weight of glycols formed by the time of reaction and the total

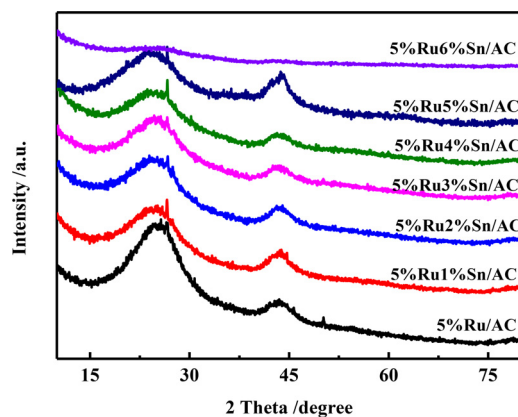


Fig. 1. XRD patterns of Ru/AC and RuSn/AC catalysts with different tin loadings.

liquid reaction volume ( $\text{g}_{\text{glycols}} \text{ L}^{-1} \text{ h}^{-1}$ ).

### 3. Results and discussion

#### 3.1. Catalyst characterization

##### 3.1.1. XRD and HRTEM of catalysts

Fig. 1 depicts the XRD patterns of Ru/AC and RuSn/AC catalysts with different tin loadings. The major diffraction peaks at 20 values of  $24.8^\circ$  and  $43.6^\circ$  can be indexed to the (003) and (101) planes of graphitized carbon (PDF #00-026-1079). No peak belonging to crystalline Ru was observed on the XRD patterns of Ru/C and RuSn/AC, indicating Ru was highly dispersed on the carbon support. Meanwhile, no peak of tin species was observed in the whole range of tin loadings, indicating tin species were also highly dispersed in the RuSn/AC catalysts.

The states of Ru and Sn particles on the catalysts were visualized by HRTEM. As shown in Fig. 2(a), Ru particles were highly dispersed with an average diameter of ca. 1.7 nm on the 5%Ru/AC catalyst. After introducing 2% and 3% of tin, the average diameter of particles slightly increased to 2.7 nm and 3.3 nm, respectively (Fig. 2b and c). No particle aggregation was found in the field of vision, as further proved by EDS

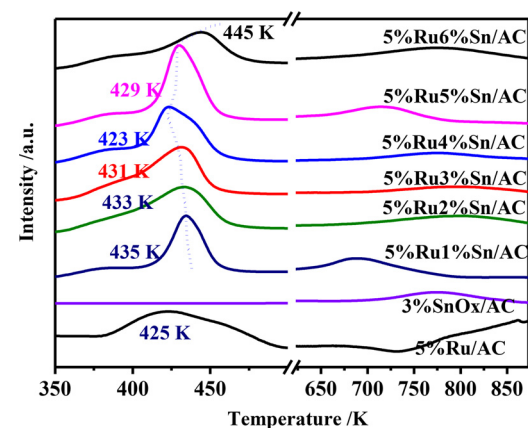


Fig. 3.  $\text{H}_2$ -TPR profiles of RuSn/AC, Ru/AC and  $\text{SnO}_x$ /AC catalysts.

elemental mappings (see supplementary information, Fig. S1). Further increasing Sn loading to 5%, in contrast, led to some particles larger than 6 nm in diameter (Fig. 2d). Moreover, the particle size has a wider distribution than that of catalysts with low Sn loadings, indicating that some of Ru and Sn species did not interact closely, and some of tin species aggregated over the 5%Ru5%Sn/AC catalyst. Correlating to the absence of diffraction peaks indexed to tin oxide or metallic tin in XRD patterns (Fig. 1), the tin species should be amorphous. The lattice spacings in the HRTEM images of 5%Ru3%Sn/AC catalyst provided more information about particles composition. As shown in Fig. 2(e and f), the lattice spacings of typical particles on 5%Ru3%Sn/AC were 0.2048, 0.2058, 0.2090 and 0.2124 nm, respectively. These lattices were not associated with metallic Ru, ruthenium oxide or tin oxide, but between those of metallic Ru and Sn. This suggests that Ru-Sn alloy was formed between Ru and Sn in the 5%Ru3%Sn/AC catalyst.

##### 3.1.2. $\text{H}_2$ -TPR of RuSn/AC catalysts

Fig. 3 presents the  $\text{H}_2$ -TPR profiles of 5%RuSn/AC catalysts with different tin loadings. For the Ru/AC catalyst, it had one main peak at 425 K, corresponding to the ruthenium reduction. At temperatures higher than 750 K, the presence of  $\text{H}_2$  consumption should be related to the methanization of carbon support by ruthenium catalysis. After the

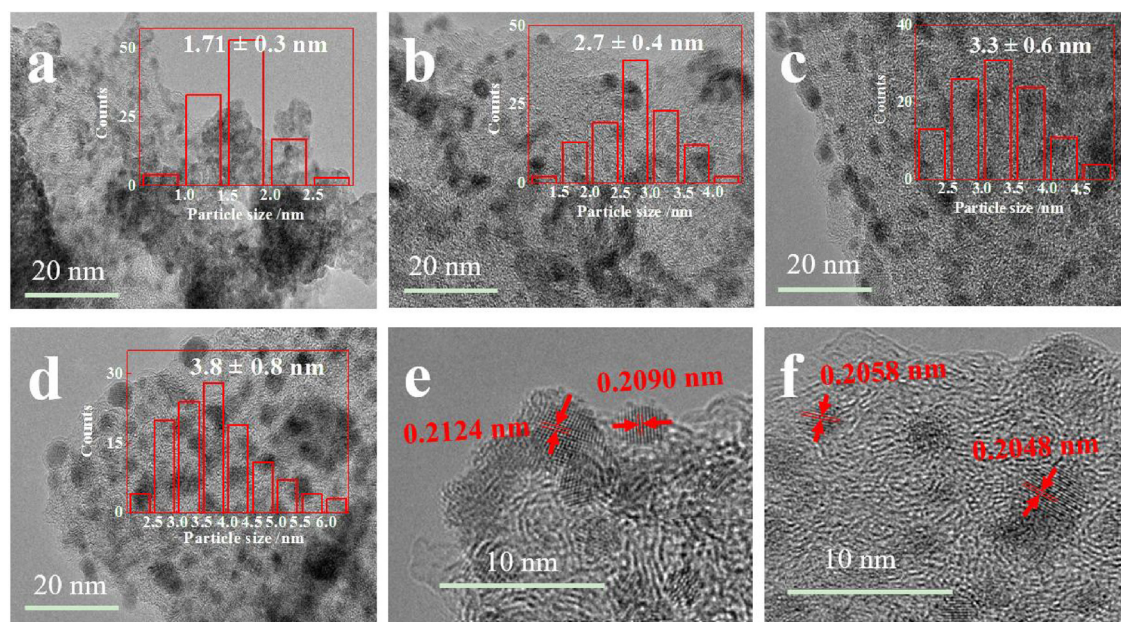


Fig. 2. HRTEM images of 5%Ru/AC (a), 5%Ru2%Sn/AC (b), 5%Ru3%Sn/AC (c, e and f) and 5%Ru5%Sn/AC (d) catalysts. The insets in the corresponding images (a-d) show the particle size frequency distribution histograms.

introduction of tin, the reduction peaks at 400–450 K varied with tin loadings. These peaks should be attributed to the reduction of Ru and tin oxides as reported elsewhere [39]. The reduction temperature gradually decreased from 435 K to 423 K as the tin loading increased from 1% to 4%. The enhanced reducibility should be related to the strong interaction between Ru and tin oxides. As reported by Deng et al., electron can transfer from metal oxides to noble metals and decrease the reduction temperatures of oxides [37]. Further increasing the tin loading to 6%, on the contrary, led to the reduction temperature of RuSn/AC catalyst increasing to 445 K. This should be ascribed to the high coverage of tin oxides over Ru particles which hindered the hydrogen activation and metal reduction. Meanwhile, an additional reduction peak appeared at 700–780 K, which is similar to that on the TPR profile of 3%SnO<sub>x</sub>/AC catalysts and should be attributed to the reduction of tin oxides [39]. The appearance of the reduction peak at high temperatures indicates that some of tin oxide species located far from the Ru particles and are difficult to be reduced in catalyst preparation [40]. It should be noted that no hydrogen consumption was observed over the 3%SnO<sub>x</sub>/AC catalyst below 523 K, indicating that the tin species are relatively stable in the absence of ruthenium and should stay as Sn<sup>4+</sup> after the catalyst preparation process. The hydrogen consumption of RuSn/AC catalysts in TPR experiments were quantified (see supplementary information, Table S1). The results demonstrated that the Ru should be totally reduced under the catalysts preparation conditions. However, the tin species at loadings > 2% were partially reduced with the reduction degree ranging from 44% to 96%. Due to the extra H<sub>2</sub> consumption by the surface functional groups on the carbon support, the reduction degrees of tin estimated by TPR would be slightly higher than the actual values (e.g., detected by XPS in Fig. 4D, as discussed in the following section).

The specific surface areas of catalysts were measured (see supplementary information Table S2). The introduction of tin to the ruthenium catalyst first slightly decreased the surface areas from 992 to ca. 832 m<sup>2</sup>/g (4% Sn loading), and then increased to 868 m<sup>2</sup>/g (6% Sn loading), which showed the same trend to the reduction temperature changes in Fig. 3. All these results indicate that the property of RuSn/AC catalysts would be notably affected by the tin loading on the catalysts. At low tin loadings (< 4%), tin interacted with ruthenium closely, whereas isolated tin oxide species were present at high tin loadings (> 5%).

The gaseous products in the TPR experiments of RuSn/AC catalysts were analyzed by *in situ* MS (see supplementary information, Fig. S2). At temperatures higher than 500 K, CO and CH<sub>4</sub> were notably formed over the 5%Ru2%Sn/AC catalyst. Differently, H<sub>2</sub>O and CO<sub>2</sub> were major products for the 5%Ru5%Sn/AC catalyst at 700–750 K. This may reflect the difference in the hydrogenation ability of catalysts. Higher yields of CO and CH<sub>4</sub> over the 5%Ru2%Sn/AC catalyst should be related to the catalytic property of metallic Ru or RuSn sites, which is more active for hydrogenation than the RuSn and Sn species on the 5%Ru5%Sn/AC catalyst.

### 3.1.3. XPS of typical RuSn/AC catalysts

Fig. 4A and B show the XPS spectra of the Ru 3p and Sn 3d core level, respectively, for RuSn/AC catalysts with different tin loadings. The binding energy of the Ru 3p<sub>3/2</sub> peak at approximately 461.9 eV was observed on the spectra of RuSn/AC catalysts, corresponding to the metallic Ru<sup>0</sup> species and accounting for ca. 30% of Ru on the catalysts. The major peak at 463.8 eV should be assigned to RuO<sub>2</sub>, which intensity gradually increased with the tin loadings [41]. The high percent of RuO<sub>2</sub> should be attributed to the oxidation of Ru during the passivation step, which is commonly adopted in the preparation process of Ru/C catalyst [42,43]. The peaks at 485.3 eV and 487.2 eV in Fig. 4B were attributed to Sn<sup>0</sup> and Sn<sup>2+/4+</sup>, respectively [44]. The percent of metallic tin gradually decreased from 25% to 10.6% when the tin loading was increased from 2% to 5%.

Pseudo *in situ* XPS characterization on the freshly reduced catalyst

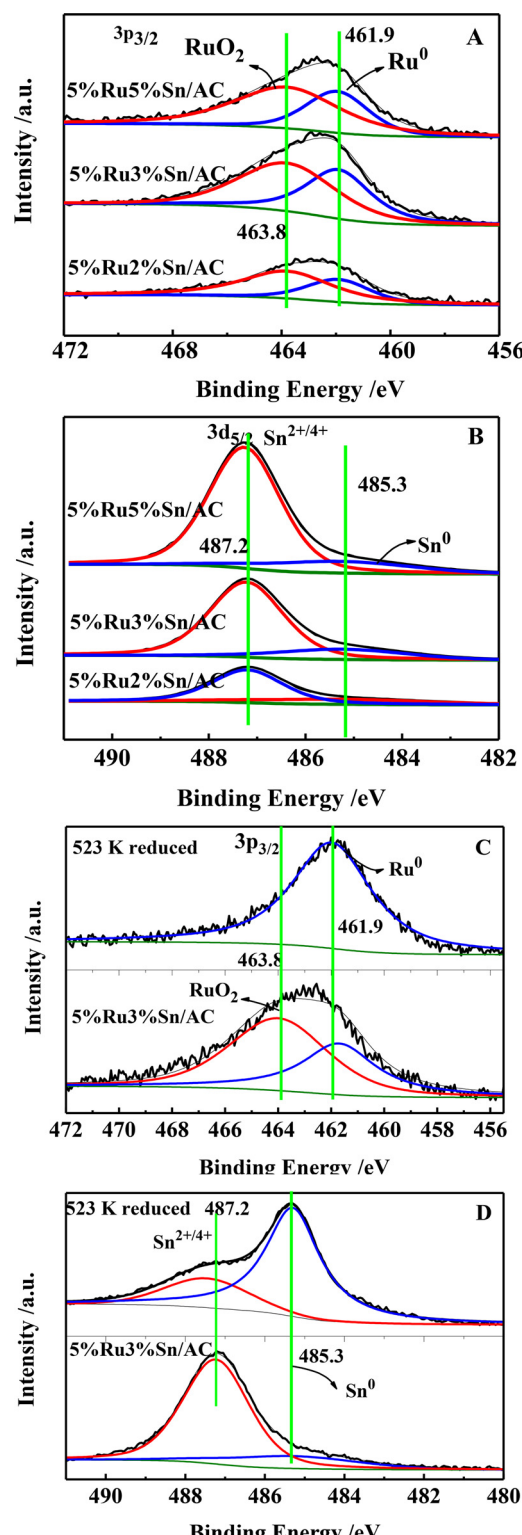


Fig. 4. XPS of RuSn/AC catalysts at different tin loadings (A and B) and 5% Ru3%Sn/AC catalysts before and after *in situ* reduction (C and D: Sn; the catalyst was reduced at 523 K in hydrogen for 2 h, and returned to room temperature to get the pseudo *in situ* spectra).

was conducted to probe the state of catalysts under reaction conditions of sugars conversion. As shown in Fig. 4C, RuO<sub>2</sub> on the as-prepared 5% Ru3%Sn/AC catalyst was completely transformed to metallic Ru after reduction, indicating that the superficial Ru oxides are prone to be reduced. Comparing the reduction temperature for pseudo *in situ* XPS

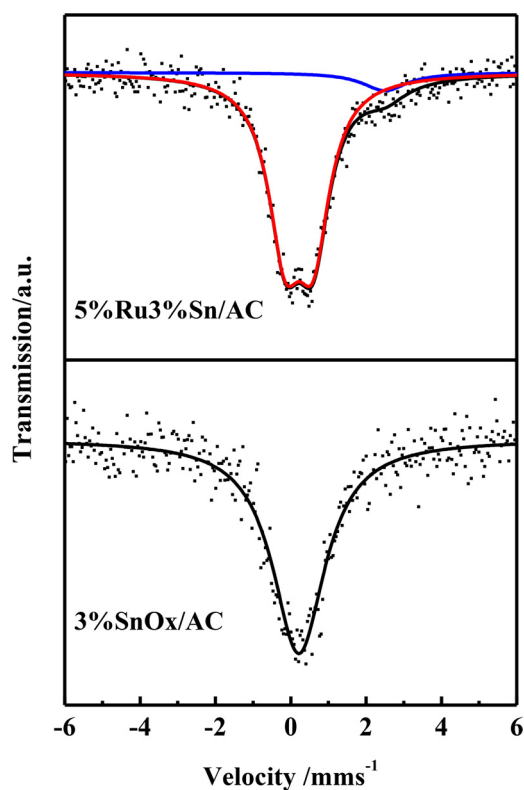


Fig. 5.  $^{119}\text{Sn}$  Mössbauer spectra of 5%Ru3%Sn/AC and 3% $\text{SnO}_x$ /AC catalysts.

characterization with the reaction conditions for sugars conversion (523 K vs. 518 K), one can speculate that the Ru should be at metallic state under reaction conditions. For the chemical state of tin, the content of metallic tin was increased from 13% to 77% in the fresh catalyst after reduction. The enhanced percent of metallic tin suggests that most tin oxide species on the 5%Ru3%Sn/AC catalyst contacted the Ru particles closely. They can be reduced during the catalytic conversion of sugars due to the facilitated hydrogen spillover from Ru particles to tin oxides, and form RuSn alloy as shown in the HRTEM analysis mentioned above. In addition, about 23% of tin oxide species were remained and might also play some catalytic roles in the reaction.

#### 3.1.4. $^{119}\text{Sn}$ Mössbauer spectra of 5%Ru3%Sn/AC and 3% $\text{SnO}_x$ /AC catalysts

To clarify the coordination environment and valence state of tin species in RuSn/AC catalysts, 5%Ru3%Sn/AC was characterized with  $^{119}\text{Sn}$  Mössbauer spectroscopy. As shown in Fig. 5, the doublet with an isomer shifts (IS) value of 0.2 was attributed to the  $\text{Sn}^{4+}$ , and the singlet with an IS value of 2.4 was attributed to the  $\text{Sn}^\circ$  in the RuSn alloy. The quadrupole splitting value for  $\text{Sn}^{4+}$  is much larger than that of bulk  $\text{SnO}_2$  (0.75 vs. 0.58 mm/s), suggesting that the tin oxides on RuSn/AC catalysts had a low symmetric geometry [35,45]. The percentages of  $\text{Sn}^\circ$  and  $\text{Sn}^{4+}$  were 13.5% and 86.5%, respectively, which is consistent with the result of XPS analysis. For the 3% $\text{SnO}_x$ /AC catalyst, the tin species had an IS value of 0, which should be attributed to  $\text{Sn}^{4+}$ . Evidently, the tin species without Ru promotion are hard to be reduced at 523 K, which is consistent with the TPR results in Fig. 3.

Correlating the preparation procedure to the results of above characterizations, it can be proposed that the chemical state of metal on the catalyst is highly related to the tin loadings and the reaction conditions. Most of tin species in the 5%Ru3%Sn/AC catalyst existed as  $\text{SnO}_2$  at a low symmetric geometry after the passivation process, and could be changed to RuSn alloy with less than 25%  $\text{SnO}_2$  left under reaction conditions of sugars conversion. At higher tin contents, more amorphous  $\text{SnO}_2$  was retained on the catalyst; it covered the RuSn alloy

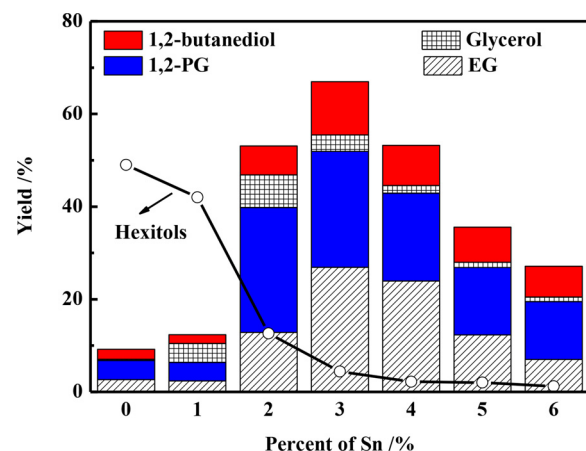


Fig. 6. Effects of tin loading on the catalytic conversion of glucose over RuSn/AC catalysts (Reaction conditions: 513 K, 5 MPa  $\text{H}_2$ , 0.35 g 5%  $\text{Rux%Sn/AC}$  catalyst, 10% glucose solution pumped for 4 min at 5 mL/min and then reacted for 10 min).

surface and decreased the hydrogenation activity.

#### 3.2. Catalytic conversion of sugars to 1,2-PG and EG

##### 3.2.1. Effects of tin loading on the activity of RuSn/AC catalysts

Since glucose is the most abundant carbohydrate, it was used as the first feedstock for catalytic evaluation. As shown in Fig. 6, the tin loading on the catalyst greatly affected the product distributions. Over the 5% Ru/AC catalyst, the primary product is hexitols at a yield of 49%, with 9% overall yield of 1,2-PG, EG and glycerol. The introduction of 3% tin significantly decreased the hexitols yield to 4.4% but increased 1,2-PG and EG yields to 25% and 26.9%, respectively, with 67% overall yield of glycols. Further increasing the tin loading to 6% caused a remarkable decrease in the glycols yield (down to 26.6%) with a notable amount of humins formation.

For glucose hydrogenation over a Ru/AC catalyst at temperatures below 473 K, sorbitol is usually the major product at a yield over 90% [46]. At elevated temperatures like 513 K in the present study, 49% yield of hexitols was obtained with 9% yield of glycols due to the hexitols hydrogenolysis [47,48]. With the modification of tin to ruthenium, the dominant product was drastically changed from hexitols to small diols of 1,2-PG and EG over the RuSn/AC catalysts. According to the reaction mechanism for glycols production in sugars conversion, three types of major reactions are involved, including isomerization, retro-aldol condensation and hydrogenation reactions [26]. Evidently, the tin species played the key role in the isomerization and retro-aldol condensation reactions. Meanwhile, the tin species may depress the hydrogenation activity of the catalyst. At low tin loadings (1% or less) in the RuSn/AC catalysts, the direct hydrogenation of glucose to sorbitol was the dominant reaction, which should be attributed to the overwhelming hydrogenation activity of the metallic Ru particles and relatively low activity of the tin species for the C–C bonds breakage. On the contrary, when tin loading was higher than 4%, as shown in the analysis of Mössbauer spectra, notable amount of amorphous  $\text{SnO}_2$  was retained on the catalyst. The tin oxide may cover the RuSn alloy surface, significantly decreased the hydrogenation activity and resulted in the humins formation. In the presence of optimal tin content (e.g., 5% Ru3%Sn/AC), the rates of three types of reactions were well balanced and high yields of glycols were obtained.

##### 3.2.2. Effects of reaction conditions on the glycols yield

Fig. 7 depicts the influence of reaction temperatures on glycols yield over the 5%Ru2%Sn/AC catalyst. At 503 K, 1,2-PG and glycerol yields were 26.7% and 11.3%, respectively, with 23.7% yield of hexitols. The

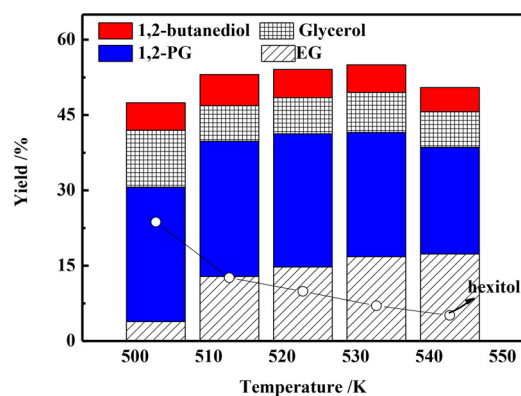


**Fig. 7.** Catalytic conversion of glucose to glycols at different reaction temperatures over the 5%Ru2%Sn/AC catalyst (Reaction conditions: 5 MPa H<sub>2</sub>, 0.35 g catalyst, 10% glucose solution pumped for 4 min at 5 mL/min and then reacted for 10 min).

hexitol yield gradually decreased with the increase of reaction temperatures, and dropped to 5.1% at 543 K. Meanwhile, the EG yield increased from 3.9% to 17.3% with a slight decrease in the 1,2-PG yield. The change of glycols yields at different temperatures is determined by the kinetics of isomerization, retro-aldol condensation and hydrogenation reactions. In general, the energy barriers for the retro-aldol condensation of sugars are notably higher than that of sugar isomerization and hydrogenation (ca. 140 kJ/mol vs. 60 kJ/mol) [49–52]. Therefore, isomerization and hydrogenation of sugars are advantaged over retro-aldol condensation at relatively low temperatures, resulting in high yields of hexitols and C<sub>3</sub> compounds (derived from fructose degradation). With the increase of reaction temperature, the contribution of glucose retro-aldol condensation was improved, causing the product selectivity shift to C<sub>2</sub> compounds.

Effects of catalysts amounts and feeding rates on glycols yield were investigated. As shown in Table 1 entry 1, EG and 1,2-PG yields was 26.9% and 25.0%, respectively, over the 5%Ru3%Sn/AC catalyst. Increasing the catalysts amount from 0.35 g to 0.5 g did not affect the

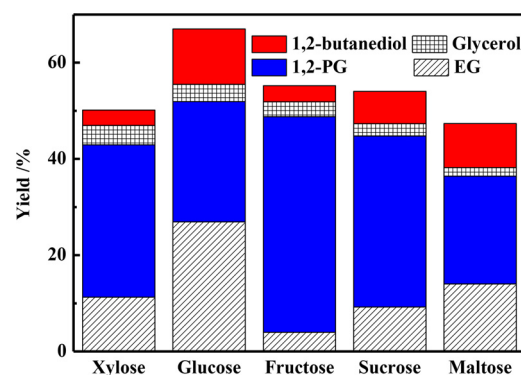


**Fig. 8.** Conversion of different sugars to glycols (Reaction conditions: 513 K, 5 MPa H<sub>2</sub>, 0.35 g 5%Ru3%Sn/AC, 10% solution, pumped for 4 min at 5 mL/min and then reacted for 10 min; Catalyst: 5%Ru3%Sn/AC).

glycols distribution (entry 2), and the overall yield of EG and 1,2-PG was kept at about 50%. This performance is confirmed by the results over the 5%Ru4%Sn/AC catalyst in entries 4–6, where the glycols yield maintained at similar values even the catalyst amounts was increased from 0.35 to 0.9 g, as shown in entries 4–6. Moreover, the glycols yield is insensitive to the feeding rate of glucose (1–10 mL/min); it levelled off at ca. 53% at feeding rates of 1 to 10 mL/min (entry 3). This should be attributed to the high activity of catalysts in C–C bonds cleavage and aldehydes hydrogenation under the present reaction conditions. Correspondingly, the volume productivity of glycols over the RuSn/AC catalysts reached ca. 180 g<sub>glycols</sub> L<sup>-1</sup> h<sup>-1</sup>, which is much higher than that in cellulosic biomass conversion at a high concentration (20 g<sub>glycols</sub> L<sup>-1</sup> h<sup>-1</sup>) [25].

### 3.2.3. Effects of feedstock on the glycols yield

Different sugars were tested for glycols production over the 5% Ru3%Sn/AC catalyst. As shown in Fig. 8, glycols distributions were highly dependent on the sugar types. For xylose conversion, yields of EG and 1,2-PG were 11.3% and 31.7%, respectively, with the EG to 1,2-PG ratio of 1:3. The ratio is about 1:1 for glucose and maltose conversion. When using fructose as the feedstock, the yield of 1,2-PG was up to 45% and the ratio of EG to 1,2-PG reached 1:10 (see supplementary information, Fig. S3). The RuSn/AC catalysts showed relatively higher selectivity toward 1,2-PG as compared with the tungsten based catalysts in the conversion of fructose based feedstock (45% vs 37%) [26,53]. Based on the reaction mechanism, the RuSn/AC catalysts would promote isomerization of glucose to fructose, which was further degraded to 1,2-PG through cascade reactions involving retro-aldol condensation and hydrogenation reactions [7,54]. To confirm this hypothesis, sucrose, a sugar consisting of equal mole of glucose and fructose, was employed for catalytic conversion. The yields of EG and 1,2-PG were 9.2% and 35.5%, respectively, with EG to 1,2-PG ratio of 1:4. From the results of different sugars conversion, one can propose that the RuSn/AC catalysts promoted the glucose isomerization to fructose, in addition to playing the key role in retro-aldol condensation and hydrogenation reactions, which caused the relatively a higher yield of 1,2-PG than EG.

### 3.2.4. Stability of the 5%Ru3%Sn/AC catalyst

The stability of the 5%Ru3%Sn/AC catalyst was tested, and the result was presented in Fig. 9. After five consecutive runs, the EG and 1,2-PG yield still reached 26.9% and 20.9%, respectively, with 63.4% yield of polyols. The slight decrease in 1,2-PG yield (ca. 4% decrease) should be attributed to the leaching of trace tin sites (ca. 4 ppm, corresponding to 1.1% of total tin in the 5%Ru3%Sn/AC catalyst), as detected by the ICP-AES. The used catalysts were then characterized by XRD and TEM (see supplementary information, Fig. S4 and Fig. S5). The used and the fresh 5%Ru3%Sn/AC catalysts showed identical XRD

**Table 1**  
Reaction results for glucose conversion over RuSn/AC catalysts under different reaction conditions<sup>a</sup>.

Entry	Catalyst	Conditions <sup>c</sup>	Yield (%) <sup>b</sup>				
			EG	1,2-PG	Gly.	1,2-BD	Hex.
1	5%Ru3%Sn/AC	0.35 g, 1 mL/min	26.9	25.0	3.6	11.5	4.4
2	5%Ru3%Sn/AC	0.5 g, 1 mL/min	27.1	21.5	2.1	9.1	3.7
3	5%Ru3%Sn/AC	0.35 g, 10 mL/min	26.9	23.5	2.2	8.0	3.6
4	5%Ru4%Sn/AC	0.35 g, 1 mL/min	24.0	18.9	1.7	8.6	2.2
5	5%Ru4%Sn/AC	0.6 g, 1 mL/min	28.5	18.3	1.5	8.3	3.2
6	5%Ru4%Sn/AC	0.9 g, 1 mL/min	28.2	17.5	1.7	7.9	3.2
7 <sup>d</sup>	5%Ru3%Sn/AC	0.35 g, 0.5 h Sorbitol	1.8	4.5	–	–	85.9
8 <sup>d</sup>	5%Ru3%Sn/AC	0.35 g, 0.5 h Mannitol	1.4	5.4	–	–	89.5

<sup>a</sup> Reaction conditions: 513 K, 5 MPa H<sub>2</sub>, 10% glucose solution, reacted for 10 min.

<sup>b</sup> EG, 1,2-PG, Gly, 1,2-BD and Hex. are abbreviations of ethylene glycol, 1,2-propylene glycol, glycerol, 1,2-butanediol and hexitols, respectively.

<sup>c</sup> the reaction conditions refer to catalyst amounts and pumping rate for entries 1–6, and sorbitol/mannitol was used as feedstock for entries 7–8; <sup>d</sup> reactions were conducted in the autoclave with one-pot process.

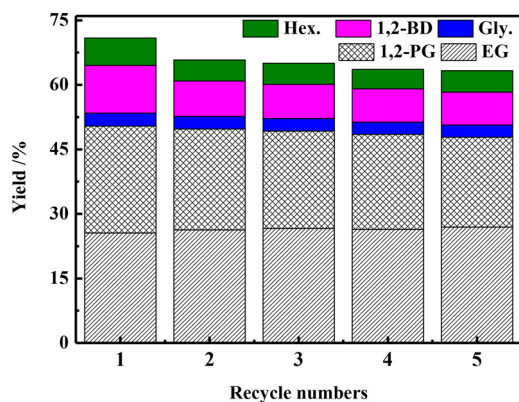


**Fig. 9.** Reusability of the 5%Ru3%Sn/AC catalyst in glucose conversion (Reaction conditions: 513 K, 5 MPa H<sub>2</sub>, 0.4 g 5%Ru3%Sn/AC, 10% solution, pumped for 4 min at 0.5 mL/min and then reacted for 10 min).

patterns, and very similar particle size distributions (average particle size: 3.4 nm vs 3.3 nm), indicating that the RuSn/AC catalyst is rather stable under reaction conditions. The chemical state of tin species in the used catalyst was revisited by <sup>119</sup>Sn Mössbauer spectroscopy (see supplementary information, Fig. S6). It is confirmed that the Sn<sup>0</sup> and Sn<sup>4+</sup> species were stable active sites for the sugar conversion.

### 3.2.5. Reaction pathways investigation

To identify the reaction pathway and the functions of different catalytic sites on the catalyst, the reaction intermediates were monitored by *in situ* sampling reactant solution during the reaction. As shown in Fig. 10(A), in the blank experiment without catalyst, the rate of glucose conversion was relatively low [55] and no polyol product was detected. In the presence of 5%Ru/AC (Fig. 10B), glucose was

100% converted in the whole time range, giving sorbitol as the main product. The yield of sorbitol reached 75% at beginning and gradually decreased to 46% with the reaction time prolonged to 10 min. The overall yield of 1,2-PG and EG was always less than 4%, indicating that the hydrogenolysis of sorbitol over the Ru/AC catalyst mainly formed other products, most likely methane and C<sub>6</sub>-C<sub>4</sub> alcohols [56,57], but did not remarkably contribute to the glycols formation, which is consistent with the results in Table 1, entries 7–8.

For the 3%SnO<sub>x</sub>/AC catalyst (Fig. 10C), the glucose conversion was enhanced as compared with the blank experiment (Fig. 10A). Glycolaldehyde, acetol and HMF were observed with maximum yields of 3.1%, 6.4% and 14.0%, respectively. As a typical product from fructose conversion, the presence of HMF at 14.0% yield indicates that glucose isomerization to fructose occurred. Correlating to the characterization results of SnO<sub>x</sub>/AC catalyst discussed above (TPR, <sup>119</sup>Sn Mössbauer spectra and XPS), it can be known that, very different from the bulk tin dioxides, the highly dispersed Sn<sup>4+</sup> species on the catalyst provide the major active sites for the glucose isomerization [32,58–60]. Additionally, they are also show activity for retro-aldol condensation of sugars in view of the glycolaldehyde and acetol formation, which are the precursors of EG and 1,2-PG [32,53].

The catalytic behavior of the RuSn/AC catalyst is shown in Fig. 10(D). EG and 1,2-PG were formed at yields of 21.0% and 26.6% in 10 min, respectively. As the precursor of 1,2-PG, acetol was present during the reaction with the yield reaching a maximum value of 16.3% at 2 min and then decreasing to 2.2% at 10 min, which was consistent with the results over Ni-SnO<sub>x</sub>/Al<sub>2</sub>O<sub>3</sub> catalysts [61]. According to the pseudo *in situ* XPS analysis discussed above, about 23% of tin on the 5% Ru3%Sn/AC catalyst would be in form of amorphous tin dioxide under the reducing reaction conditions. Correlating to the result in Fig. 10(C), the highly dispersed Sn<sup>4+</sup> species promoted the glucose isomerization [60]. In the followed reaction step, considering that the amount of tin in RuSn alloy is notably higher than that of tin oxide, the former should

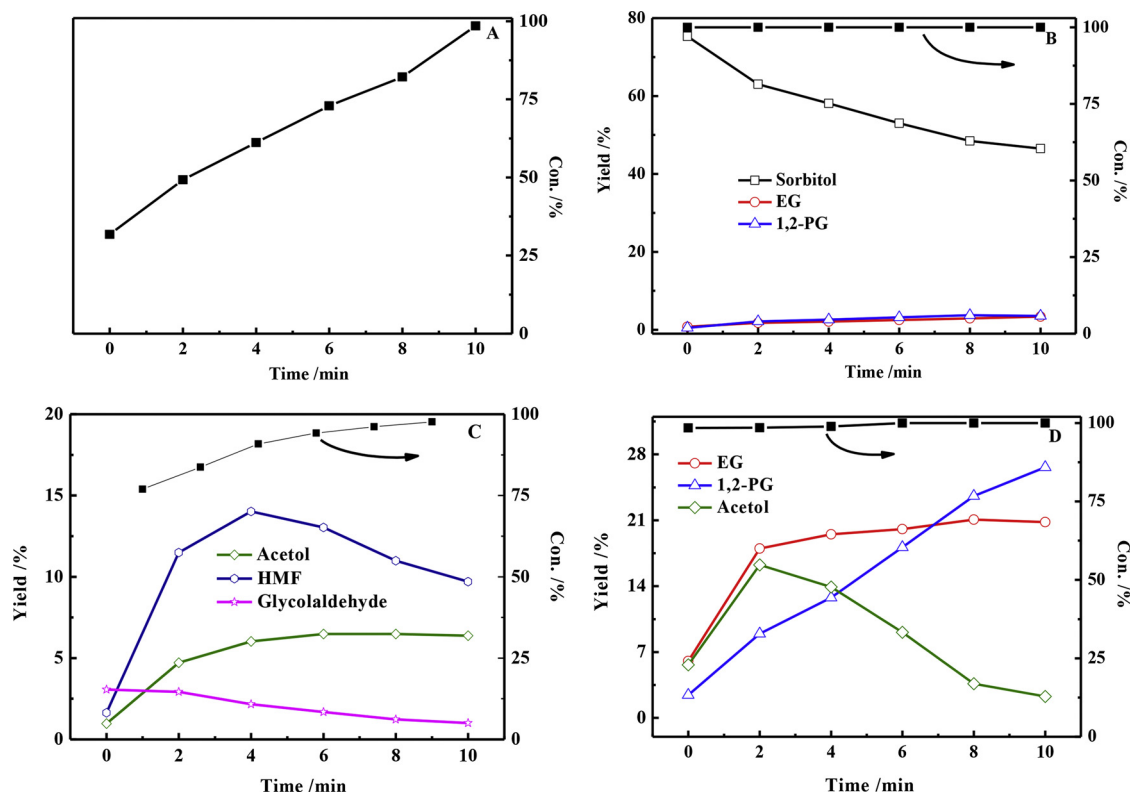
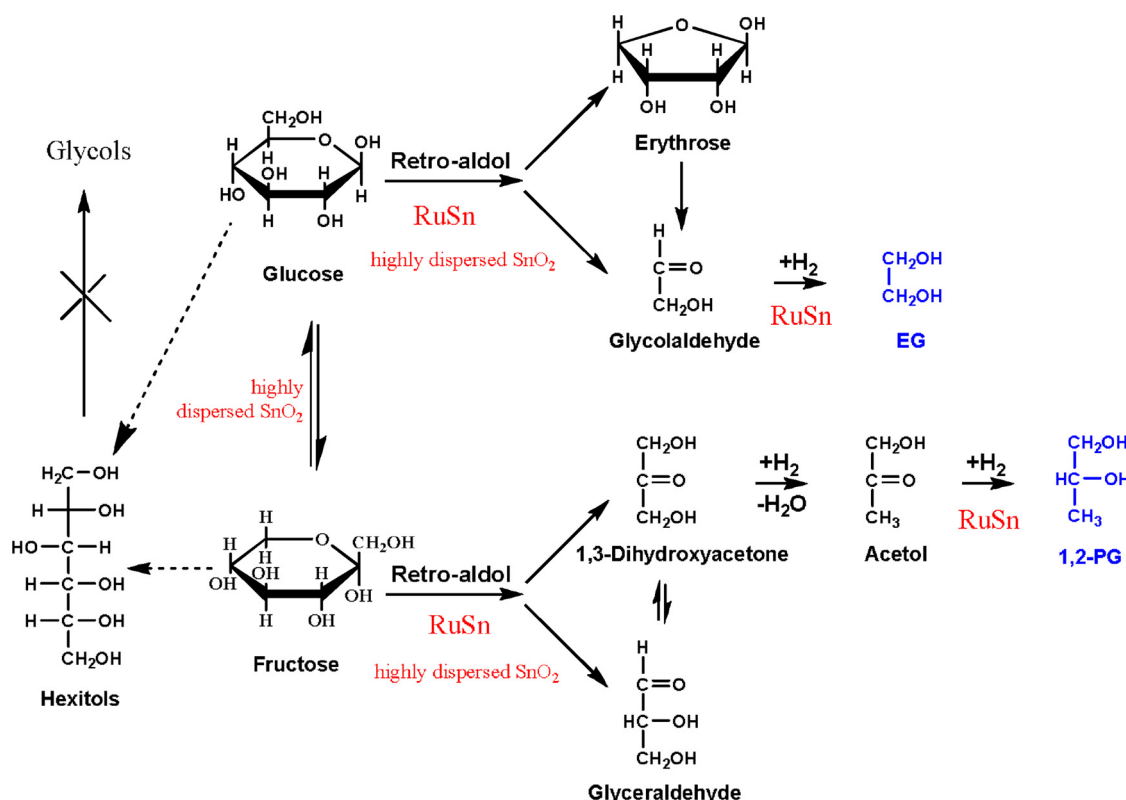


**Fig. 10.** Products distributions in glucose conversion over different catalysts: blank test without catalyst (A), 5%Ru/AC (B), 3%SnO<sub>x</sub>/AC (C), 5%Ru3%Sn/AC (D) (Reaction conditions: 513 K, 5 MPa H<sub>2</sub>, 0.35 g catalyst, 10% glucose solution, 5 mL/min, pumped for 4 min and sampling the product every 2 min, the start sampling time is considered to be 0, HMF: 5-hydroxymethyl furfural).



**Scheme 1.** Reaction scheme for conversion of sugars to glycols over RuSn/AC catalysts.

play the dominant role in the retro-aldol condensation. Therefore, both the 77% of tin in RuSn alloy and the highly dispersed  $\text{Sn}^{4+}$  species catalyzed retro-aldol condensation of sugars to form  $\text{C}_2$  and  $\text{C}_3$  intermediates, which were finally hydrogenated over RuSn sites to form EG and 1,2-PG.

According to the reaction intermediates in conditional experiments and the catalyst structures, the reaction pathways over typical catalysts are proposed in **Scheme 1**. Highly dispersed amorphous tin dioxide catalyzes glucose isomerization. The produced fructose and unreacted glucose are further degraded via the retro-aldol condensation on the sites of metallic Sn in RuSn alloy and highly dispersed  $\text{Sn}^{4+}$  on the catalysts. Finally, the  $\text{C}_2$  and  $\text{C}_3$  intermediates of glycolaldehyde and acetol are hydrogenated over RuSn alloy sites to produce 1,2-PG and EG. Additionally, hexitols are rather stable under the present reaction conditions and do not contribute to the glycols production.

#### 4. Conclusions

Tin modified Ru/AC catalysts were synthesized for converting sugars to glycols in a semi-continuous autoclave. The tin loading greatly affected the structure of catalyst. Bimetallic RuSn alloy was formed and small amounts of highly dispersed amorphous tin dioxide when tin loading was less than 4%. At tin contents higher than 5%, the RuSn alloy particles was covered with more  $\text{SnO}_2$  species. Over the optimal 5%Ru3%Sn/AC catalyst, 77% tin existed in the RuSn alloy with 23% of tin present as tin dioxide under reducing environment of the reaction conditions for sugars conversion.

In catalytic conversion of 10% glucose at 513 K for 10 min, the yield of 1,2-PG and EG reached 25% and 26.9%, respectively, with the overall yield of glycols reaching 67% over the 5%Ru3%Sn/AC catalyst. The feeding rate of glucose can be increased from 1 to 10 mL/min without depressing the glycols yield, and the glycols productivity reached  $180 \text{ g L}^{-1} \text{ h}^{-1}$ . The reaction networks and the roles of tin in the reaction were proposed according to conditional experiments and

catalysts characterizations. The highly dispersed  $\text{SnO}_2$  promotes the glucose isomerization and partially takes part in retro-aldol condensation of sugars. The produced fructose and unreacted glucose are transformed to EG and 1,2-PG mainly over the RuSn alloy via retro-aldol condensation and hydrogenation reactions. Over the 5%Ru3%Sn/AC catalyst, the rates of glucose isomerization, retro-aldol condensation and hydrogenation reactions are balanced to give a high yield of 1,2-PG and EG.

#### Acknowledgements

This work was supported by the National Science Foundation of China (21306191, 21376239, 21690081, 21690084 and 21776268), "Transformational Technologies for Clean Energy and Demonstration", Strategic Priority Research Program of the Chinese Academy of Sciences, Grant No. XDA 21060200. We also thank Xiaoli Pan for the HRTEM characterizations. Jifeng Pang acknowledges the support from China Scholarship Council for the Visiting Scholars Program (File No. 201704910436).

#### Appendix A. Supplementary data

Supplementary material related to this article can be found, in the online version, at doi:<https://doi.org/10.1016/j.apcatb.2018.08.022>.

#### References

- [1] J. Pang, M. Zheng, R. Sun, A. Wang, X. Wang, T. Zhang, Synthesis of ethylene glycol and terephthalic acid from biomass for producing PET, *Green Chem.* 18 (2016) 342–359.
- [2] H. Yue, Y. Zhao, X. Ma, J. Gong, Ethylene glycol: properties, synthesis, and applications, *Chem. Soc. Rev.* 41 (2012) 4218–4244.
- [3] G.W. Huber, S. Iborra, A. Corma, Synthesis of transportation fuels from biomasses: chemistry, catalysts, and engineering, *Chem. Rev.* 106 (2006) 4044–4098.
- [4] A.M. Ruppert, K. Weinberg, R. Palkovits, Hydrogenolysis goes bio: from carbohydrates and sugar alcohols to platform chemicals, *Angew. Chem. Int. Ed.* 51 (2012) 2564–2601.

- [5] J.S. Luterbacher, D.M. Alonso, J.A. Dumesic, Targeted chemical upgrading of lignocellulosic biomass to platform molecules, *Green Chem.* 16 (2014) 4816–4838.
- [6] M.J. Climent, A. Corma, S. Iborra, Conversion of biomass platform molecules into fuel additives and liquid hydrocarbon fuels, *Green Chem.* 16 (2014) 516–547.
- [7] A. Wang, T. Zhang, One-pot conversion of cellulose to ethylene glycol with multi-functional tungsten-based catalysts, *Acc. Chem. Res.* 46 (2013) 1377.
- [8] M. Zheng, J. Pang, R. Sun, A. Wang, T. Zhang, Selectivity control for cellulose to diols: dancing on eggs, *ACS Catal.* 7 (2017) 1939–1954.
- [9] N. Ji, T. Zhang, M. Zheng, A. Wang, H. Wang, X. Wang, J.G. Chen, Direct catalytic conversion of cellulose into ethylene glycol using nickel-promoted tungsten carbide catalysts, *Angew. Chem. Int. Ed.* 47 (2008) 8510–8513.
- [10] M.Y. Zheng, A.Q. Wang, N. Ji, J.F. Pang, X.D. Wang, T. Zhang, Transition metal-tungsten bimetallic catalysts for the conversion of cellulose into ethylene glycol, *ChemSusChem* 3 (2010) 63–66.
- [11] Y. Zhang, A. Wang, T. Zhang, A new 3D mesoporous carbon replicated from commercial silica as a catalyst support for direct conversion of cellulose into ethylene glycol, *Chem. Commun.* 46 (2010) 862–864.
- [12] N. Li, Y. Zheng, L. Wei, H. Teng, J. Zhou, Metal nanoparticles supported on  $WO_3$  nanosheets for highly selective hydrogenolysis of cellulose to ethylene glycol, *Green Chem.* 19 (2017) 682–691.
- [13] M.S. Hamdy, M.A. Eissa, S.M.A.S. Keshk, New catalyst with multiple active sites for selective hydrogenolysis of cellulose to ethylene glycol, *Green Chem.* 19 (2017) 5144–5151.
- [14] Z. Tai, J. Zhang, A. Wang, M. Zheng, T. Zhang, Temperature-controlled phase-transfer catalysis for ethylene glycol production from cellulose, *Chem. Commun.* 48 (2012) 7052–7054.
- [15] Z. Tai, J. Zhang, A. Wang, J. Pang, M. Zheng, T. Zhang, Catalytic conversion of cellulose to ethylene glycol over a low-cost binary catalyst of Raney Ni and tungstic acid, *ChemSusChem* 6 (2013) 652–658.
- [16] Y. Liu, C. Luo, H. Liu, Tungsten trioxide promoted selective conversion of cellulose into propylene glycol and ethylene glycol on a ruthenium catalyst, *Angew. Chem. Int. Ed.* 51 (2012) 3249–3253.
- [17] X. Wang, L. Meng, F. Wu, Y. Jiang, L. Wang, X. Mu, Efficient conversion of microcrystalline cellulose to 1,2-alkanediols over supported Ni catalysts, *Green Chem.* 14 (2012) 758–765.
- [18] Z. Xiao, S. Jin, M. Pang, C. Liang, Conversion of highly concentrated cellulose to 1,2-propanediol and ethylene glycol over highly efficient CuCr catalysts, *Green Chem.* 15 (2013) 891–895.
- [19] R. Sun, T. Wang, M. Zheng, W. Deng, J. Pang, A. Wang, X. Wang, T. Zhang, Versatile nickel–lanthanum(III) catalyst for direct conversion of cellulose to glycols, *ACS Catal.* (2014) 874–883.
- [20] J. Xi, D. Ding, Y. Shao, X. Liu, G. Lu, Y. Wang, Production of ethylene glycol and its monoether derivative from cellulose, *ACS Sust. Chem. Eng.* 2 (2014) 2355–2362.
- [21] P. Kumar, D.M. Barrett, M.J. Delwiche, P. Stroeve, Methods for pretreatment of lignocellulosic biomass for efficient hydrolysis and biofuel production, *Ind. Eng. Chem. Res.* 48 (2009) 3713–3729.
- [22] J. Pang, M. Zheng, R. Sun, L. Song, A. Wang, X. Wang, T. Zhang, Catalytic conversion of cellulosic biomass to ethylene glycol: effects of inorganic impurities in biomass, *Bioresour. Technol.* 175 (2015) 424–429.
- [23] W. Deng, Q. Zhang, Y. Wang, Catalytic transformation of cellulose and its derived carbohydrates into chemicals involving C–C bond cleavage, *J. Energy Chem.* 24 (2015) 595–607.
- [24] M.J. Climent, A. Corma, S. Iborra, Converting carbohydrates to bulk chemicals and fine chemicals over heterogeneous catalysts, *Green Chem.* 13 (2011) 520–540.
- [25] J. Pang, M. Zheng, A. Wang, R. Sun, H. Wang, Y. Jiang, T. Zhang, Catalytic conversion of concentrated miscanthus in water for ethylene glycol production, *AIChE J.* 60 (2014) 2254–2262.
- [26] G. Zhao, M. Zheng, J. Zhang, A. Wang, T. Zhang, Catalytic conversion of concentrated glucose to ethylene glycol with semicontinuous reaction system, *Ind. Eng. Chem. Res.* 52 (2013) 9566–9572.
- [27] R. Ooms, M. Dusselier, J.A. Geboers, B. Op de Beeck, R. Verhaeveren, E. Gobechiaya, J. Martens, A. Redl, B.F. Sels, Conversion of sugars to ethylene glycol with nickel tungsten carbide in a fed-batch reactor: high productivity and reaction network elucidation, *Green Chem.* 16 (2013) 695–707.
- [28] C. Liu, C. Zhang, S. Sun, K. Liu, S. Hao, J. Xu, Y. Zhu, Y. Li, Effect of  $WO_x$  on bifunctional Pd– $WO_x$ /Al<sub>2</sub>O<sub>3</sub> catalysts for the selective hydrogenolysis of glucose to 1,2-propanediol, *ACS Catal.* 5 (2015) 4612–4623.
- [29] C. Liu, C. Zhang, S. Hao, S. Sun, K. Liu, J. Xu, Y. Zhu, Y. Li,  $WO_x$  modified Cu/Al<sub>2</sub>O<sub>3</sub> as a high-performance catalyst for the hydrogenolysis of glucose to 1,2-propanediol, *Catal. Today* 261 (2016) 116–127.
- [30] Z. Xiao, S. Jin, G. Sha, C.T. Williams, C. Liang, Two-step conversion of biomass-derived glucose with high concentration over Cu–Cr catalysts, *Ind. Eng. Chem. Res.* 53 (2014) 8735–8743.
- [31] J. Wang, G. Yao, Y. Wang, H. Zhang, Z. Huo, F. Jin, A novel Pd/C-catalyzed conversion of glucose to 1,2-propanediol by water splitting with Zn, *RSC Adv.* 5 (2015) 51435–51439.
- [32] M.S. Holm, S. Saravananurugan, E. Taarning, Conversion of sugars to lactic acid derivatives using heterogeneous zeotype catalysts, *Science* 328 (2010) 602–605.
- [33] L. Ren, Q. Guo, P. Kumar, M. Orazov, D. Xu, S.M. Alhassan, K.A. Mkhoyan, M.E. Davis, M. Tsapatsis, Self-pillared, single-unit-cell Sn-MFI zeolite nanosheets and their use for glucose and lactose isomerization, *Angew. Chem. Int. Ed.* 54 (2015) 10848–10851.
- [34] F. de Clippele, M. Dusselier, R. Van Rompaey, P. Vanelderen, J. Dijkmans, E. Makshina, L. Giebel, S. Oswald, G.V. Baron, J.F.M. Denayer, P.P. Pescarmona, P.A. Jacobs, B.F. Sels, Fast and selective sugar conversion to alkyl lactate and lactic acid with bifunctional carbon–silica catalysts, *J. Am. Chem. Soc.* 134 (2012) 10089–10101.
- [35] J. Pang, M. Zheng, X. Li, L. Song, R. Sun, J. Sebastian, A. Wang, J. Wang, X. Wang, T. Zhang, Catalytic conversion of carbohydrates to methyl lactate using isolated tin sites in SBA-15, *ChemistrySelect* 2 (2017) 309–314.
- [36] R. De Clercq, M. Dusselier, B.F. Sels, Heterogeneous catalysis for bio-based polyester monomers from cellulosic biomass: advances, challenges and prospects, *Green Chem.* 19 (2017) 5012–5040.
- [37] T. Deng, H. Liu, Promoting effect of  $SnO_x$  on selective conversion of cellulose to polyols over bimetallic Pt– $SnO_x$ /Al<sub>2</sub>O<sub>3</sub> catalysts, *Green Chem.* 15 (2013) 116–124.
- [38] R. Sun, M. Zheng, J. Pang, X. Liu, J. Wang, X. Pan, A. Wang, X. Wang, T. Zhang, Selectivity-switchable conversion of cellulose to glycols over Ni–Sn catalysts, *ACS Catal.* 6 (2016) 191–201.
- [39] S.G. Wettstein, J.Q. Bond, D.M. Alonso, H.N. Pham, A.K. Datye, J.A. Dumesic, RuSn bimetallic catalysts for selective hydrogenation of levulinic acid to gamma-valerolactone, *Appl. Catal. B Environ.* 117–118 (2012) 321–329.
- [40] Md.C. Aguirre, P. Reyes, M. Oporto, I. Melián-Cabrera, J.L.G. Fierro, Liquid phase hydrogenation of crotonaldehyde over bimetallic Rh–Sn/SiO<sub>2</sub> catalysts: effect of the Sn/Rh ratio, *Appl. Catal. A Gen.* 233 (2002) 183–196.
- [41] A. Velázquez-Palenzuela, E. Brillas, C. Arias, F. Centellas, J.A. Garrido, R.M. Rodríguez, P.-L. Cabot, Structural characterization of Ru-modified carbon-supported Pt nanoparticles using spontaneous deposition with CO oxidation activity, *J. Phys. Chem. C* 116 (2012) 18469–18478.
- [42] H. Kobayashi, H. Matsuhashi, T. Komanoya, K. Hara, A. Fukuoka, Transfer hydrogenation of cellulose to sugar alcohols over supported ruthenium catalysts, *Chem. Commun.* 47 (2011) 2366–2368.
- [43] D.R. Vardon, A.E. Settle, V. Vorotnikov, M.J. Menart, T.R. Eaton, K.A. Unocic, K.X. Steirer, K.N. Wood, N.S. Cleveland, K.E. Moyer, W.E. Michener, G.T. Beckham, Ru–Sn/AC for the aqueous-phase reduction of succinic acid to 1,4-butanediol under continuous process conditions, *ACS Catal.* 7 (2017) 6207–6219.
- [44] Z. Zhu, Z. Lu, B. Li, S. Guo, Characterization of bimetallic Ru–Sn supported catalysts and hydrogenation of 1,4-cyclohexanedicarboxylic acid, *Appl. Catal. A Gen.* 302 (2006) 208–214.
- [45] X. Li, K. Zhu, J. Pang, M. Tian, J. Liu, A.I. Rykov, M. Zheng, X. Wang, X. Zhu, Y. Huang, B. Liu, J. Wang, W. Yang, T. Zhang, Unique role of Mössbauer spectroscopy in assessing structural features of heterogeneous catalysts, *Appl. Catal. B Environ.* 224 (2018) 518–532.
- [46] B.W. Hoffer, E. Crezee, P.R.M. Mooijman, A.D. van Langeveld, F. Kapteijn, J.A. Moulijn, Carbon supported Ru catalysts as promising alternative for Raney-type Ni in the selective hydrogenation of d-glucose, *Catal. Today* 79–80 (2003) 35–41.
- [47] J. Pang, A. Wang, M. Zheng, Y. Zhang, Y. Huang, X. Chen, T. Zhang, Catalytic conversion of cellulose to hexitols with mesoporous carbon supported Ni-based bimetallic catalysts, *Green Chem.* 14 (2012) 614–617.
- [48] S. Tronci, B. Pittau, Conversion of glucose and sorbitol in the presence of Ru/C and Pt/C catalysts, *RSC Adv.* 5 (2015) 23086–23093.
- [49] J. Zhang, B. Hou, A. Wang, Z. Li, H. Wang, T. Zhang, Kinetic study of the competitive hydrogenation of glycolaldehyde and glucose on Ru/C with or without AMT, *AIChE J.* 61 (2015) 224–238.
- [50] G. Zhao, M. Zheng, R. Sun, Z. Tai, J. Pang, A. Wang, X. Wang, T. Zhang, Ethylene glycol production from glucose over W–Ru catalysts: maximizing yield by kinetic modeling and simulation, *AIChE J.* 63 (2017) 2072–2080.
- [51] B.M. Kabyemela, T. Adschari, R.M. Malaluan, K. Arai, Kinetics of glucose epimerization and decomposition in subcritical and supercritical water, *Ind. Eng. Chem. Res.* 36 (1997) 1552–1558.
- [52] M.Y. Zheng, A.Q. Wang, J.F. Pang, N. Li, T. Zhang, Reaction pathways and mechanisms in thermocatalytic biomass conversion I: cellulose structure, in: M. Schaf, Z.C. Zhang (Eds.), *Depolymerization and Conversion by Heterogeneous Catalysts*, 2016, pp. 227–260.
- [53] L. Zhou, A. Wang, C. Li, M. Zheng, T. Zhang, Selective production of 1,2-propylene glycol from Jerusalem Artichoke tuber using Ni–W<sub>2</sub>C/AC catalysts, *ChemSusChem* 5 (2012) 932–938.
- [54] M. Zheng, J. Pang, A. Wang, T. Zhang, One-pot catalytic conversion of cellulose to ethylene glycol and other chemicals: from fundamental discovery to potential commercialization, *Chin. J. Catal.* 35 (2014) 602–613.
- [55] B.M. Kabyemela, T. Adschari, R.M. Malaluan, K. Arai, Glucose and fructose decomposition in subcritical and supercritical water: detailed reaction pathway, mechanisms, and kinetics, *Ind. Eng. Chem. Res.* 38 (1999) 2888–2895.
- [56] M.F.N. D'Angelo, V. Ordovsky, J. van der Schaaf, J.C. Schouten, T.A. Nijhuis, Selective production of methane from aqueous biocarbohydrate streams over a mixture of platinum and ruthenium catalysts, *ChemSusChem* 7 (2014) 627–630.
- [57] I. Murillo Leo, M. López Granados, J.L.G. Fierro, R. Mariscal, Selective conversion of sorbitol to glycols and stability of nickel–ruthenium supported on calcium hydroxide catalysts, *Appl. Catal. B Environ.* 185 (2016) 141–149.
- [58] Y. Roman-Leshkov, M. Moliner, J.A. Labinger, M.E. Davis, Mechanism of glucose isomerization using a solid lewis acid catalyst in water, *Angew. Chem. Int. Ed.* 49 (2010) 8954–8957.
- [59] A.A. Rosatella, S.P. Simeonov, R.F.M. Frade, C.A.M. Afonso, 5-Hydroxymethylfurfural (HMF) as a building block platform: biological properties, synthesis and synthetic applications, *Green Chem.* 13 (2011) 754–793.
- [60] Q. Hou, M. Zhen, L. Liu, Y. Chen, F. Huang, S. Zhang, W. Li, M. Ju, Tin phosphate as a heterogeneous catalyst for efficient dehydration of glucose into 5-hydroxymethylfurfural in ionic liquid, *Appl. Catal. B Environ.* 224 (2018) 183–193.
- [61] T. Deng, H. Liu, Direct conversion of cellulose into acetol on bimetallic Ni– $SnO_x$ /Al<sub>2</sub>O<sub>3</sub> catalysts, *J. Mol. Catal. A Chem.* 388–389 (2014) 66–73.